


ORIGINAL ARTICLE

Open Access



Optimizing Multi-Row Cam Roller Bearing for Long Fatigue Life of Hydraulic Motors

Yu Fang¹, Qi Su^{1*}, Pengpeng Dong², Yu Yang³, Bing Xu¹, Chao Zhang¹ and Junhui Zhang^{1*} 

Abstract

Cam-lobe radial-piston hydraulic motors are widely used as rotation driving units for various marine machinery owing to their ultrahigh output torque (more than 100 kN m). A multi-row cam roller bearing (MCRB) is the key component that directly determines the fatigue life of a cam-lobe radial-piston hydraulic motor. However, compact geometry and complex loads render MCRB susceptible to fatigue failure, highlighting the need for an optimized MCRB to achieve longer fatigue life and higher reliability. Therefore, this study proposes an innovative geometry optimization method for an MCRB to improve its fatigue life. In this method, a quasi-static model was developed to calculate the load distribution, with the fatigue life of the MCRB calculated using both basic dynamic loading and load distribution. Subsequently, a genetic algorithm was used to obtain the optimized geometry parameters, which significantly improved the fatigue life of the MCRB. Finally, a loading test was conducted on a hydraulic motor installed with both the initial and optimized MCRB to validate the effectiveness of the proposed optimization method. This study provides a theoretical guideline for optimizing the design of MCRB, thereby increasing the fatigue life of hydraulic motors.

Keywords Hydraulic motor, Cam roller bearing, Fatigue life, Geometry optimization, Load distribution

1 Introduction

Cam-lobe radial-piston hydraulic motors are low-speed and high-torque hydraulic motors widely used as rotation driving units in various large machinery such as deck winches, tunnel boring machines, and dredgers [1–3]. In marine applications, particularly those involving tough winches, this type of hydraulic motor is renowned for delivering superior torque control at any speed, thereby minimizing the risk of seizures and malfunctions. As the most important power transmission component in a

hydraulic motor, a multi-row cam roller bearing (MCRB) can directly convert hydraulic energy into rotating mechanical energy. However, an MCRB operates with a compact geometry and high load, rendering it prone to fatigue failure [4, 5]. Generally, the MCRB is the first to fail in a hydraulic motor, which directly determines the fatigue life of the hydraulic motor. The fatigue life of an MCRB mainly depends on the basic dynamic load rating and load distribution [6]—all determined by geometric parameters. As a result, designing an MCRB with an optimized geometry to achieve a long fatigue life and high reliability of hydraulic motors is crucial.

The finite element method (FEM) and analytical method are two widely used methods to calculate the load distribution in rolling element bearings [7]. The FEM can easily accommodate all the components of the bearings, shafts, and supporting structures and obtain accurate results. Kania [8] used the FEM to calculate the roller deformation in a slewing bearing. Demirhan and Kanber [9] obtained stress and displacement distributions in

*Correspondence:

Qi Su

suqi@zju.edu.cn

Junhui Zhang

benzjh@zju.edu.cn

¹ State Key Laboratory of Fluid Power and Mechatronic Systems, Department of Mechanical Engineering, Zhejiang University, Hangzhou 310027, China

² Hangzhou Applied Acoustics Research Institute, Hangzhou 310027, China

³ Zenmax Hydraulics Co., Ltd., Qinhuangdao 066000, China



© The Author(s) 2024. **Open Access** This article is licensed under a Creative Commons Attribution 4.0 International License, which permits use, sharing, adaptation, distribution and reproduction in any medium or format, as long as you give appropriate credit to the original author(s) and the source, provide a link to the Creative Commons licence, and indicate if changes were made. The images or other third party material in this article are included in the article's Creative Commons licence, unless indicated otherwise in a credit line to the material. If material is not included in the article's Creative Commons licence and your intended use is not permitted by statutory regulation or exceeds the permitted use, you will need to obtain permission directly from the copyright holder. To view a copy of this licence, visit <http://creativecommons.org/licenses/by/4.0/>.

cylindrical roller-bearing rings and experimentally validated their FEM solutions. Lostado et al. [10] determined the contact stresses in double-row tapered roller bearings using the FEM, which was validated and adjusted using an analytical method and contact pressure sensor experiment. However, FEM incurs high computational costs and requires a denser mesh in the contact area, leading to extremely low computational efficiency. Moreover, FEM has poor flexibility, making it difficult to adjust the geometry and process the results immediately. As a result, the FEM is unsuitable for the continuous optimization of the MCRB. In contrast to the FEM, the analytical method based on quasi-static analysis has higher computational efficiency and greater flexibility. Jones [11] developed a general theory for the load-deflection analysis of bearings based on the Hertz theory. Harris and Kotzalas [12] improved the model by applying a widely known slicing technique; as a result, the model could analyze the roller contact along the axial direction under misalignment and heavily loaded conditions. Analytical methods have been used to calculate the load distributions in cylinder roller bearings [13], tapered roller bearings [14, 15], double-row tapered roller bearings [16], and ball bearings [17–19].

Although numerous studies have focused on load distribution in various rolling bearings, research that considers the influence of geometric variations on load distribution when optimizing rolling bearings remains limited. Most studies focused on maximizing the basic dynamic load rating to prolong fatigue life [20–22]. Various types of optimization algorithms, including genetic algorithms [23, 24], evolutionary algorithms [25–27], metaheuristic algorithms [21], and hybrid algorithms [20, 28, 29], have been utilized to achieve optimal geometry

parameters for higher computing efficiency. In addition, the EHL film thickness [22], friction torque [30], and bearing stiffness [31] are considered constraints or other objective functions. Compared with traditional rolling element bearings, the outer rings of MCRB are prone to free tilting and flexible deformation, which can significantly alter the load distribution [32]. In this study, a geometry optimization method that considers both the dynamic load rating and load distribution is proposed to obtain a longer fatigue life for MCRB.

The remainder of this paper is organized as follows. Section 2 introduces the working principles and failure modes of the MCRB in hydraulic motors. Subsequently, a geometry optimization method is proposed in Section 3. Based on this method, the optimized geometric parameters of the MCRB were obtained and discussed in Section 4. Finally, a comparative experiment between the initial and optimized MCRB was conducted on a hydraulic motor test bench to validate the effectiveness of the proposed optimization method.

2 Working Principle and Failure Analysis of MCRB

Figure 1 shows the structural diagram of the cam-lobe radial-piston hydraulic motor. In this motor, the cylinder block and guide plates are fixed, whereas the piston assemblies reciprocate in the cylinder block to convert hydraulic power into mechanical torque. The working principle of the hydraulic motor is as follows. When the piston chamber is connected to the high-pressure oil port on the oil distributor, the high-pressure oil enters the piston chamber to push the piston assembly outward to rotate the cam ring. When the piston chamber passes the high-pressure oil port and connects to the

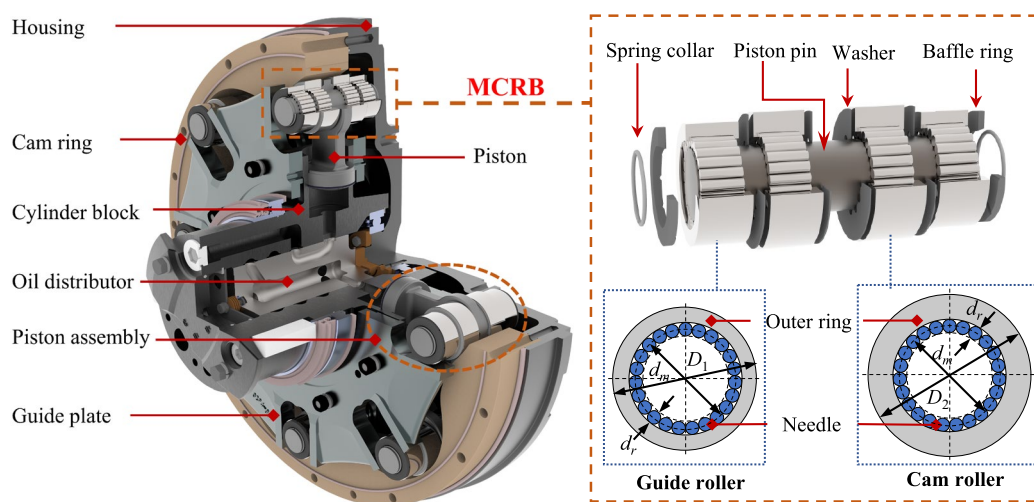


Figure 1 Structure diagram of cam-lobe radial-piston hydraulic motor and MCRB

low-pressure oil port on the oil distributor, the cam ring rotates to press the piston assembly inward to drain the hydraulic oil from the low-pressure oil port. The hydraulic motor can output continuous rotation when the cyclic movement is repeated. The MCRB on the piston assembly is a crucial transmission component that endures complex loads owing to its composition of two guide rollers and two cam rollers. The cam and guide rollers are all full complement needle bearings and possess the same pitch diameter d_m and needle diameter d_r . The outer ring diameter of the guide roller D_1 is smaller than that of the cam roller D_2 .

A typical failed piston assembly disassembled from a failed hydraulic motor is shown in Figure 2. The failed motor served in the deck winch for approximately three years. The red dashed rectangles marked on the piston pin represent severe fatigue wear regions in contact with the needles of the cam rollers. The needle in the cam roller in Figure 2 exhibits a large amount of fatigue pitting, indicating that the fatigue severity on the needle is comparatively lower than that observed on the piston pin. The outer ring of the cam roller in Figure 2 shows almost no wear scarring, suggesting that the contact pressure on the outer ring is much smaller than that on the piston pin, thus indicating that the fatigue of the MCRB causes the failure of the

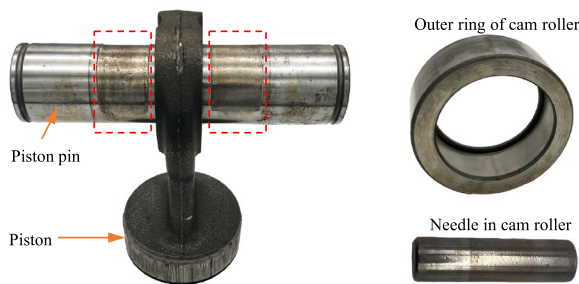


Figure 2 Failure piston assembly

piston assembly, with the cam roller most susceptible to fatigue failure in the MCRB. Hence, optimizing the geometric parameters of MCRB for a longer fatigue life is necessary.

3 Geometry Optimization Method of MCRB

In this section, the geometry optimization method, which comprises quasi-static and optimization models, is introduced. A quasi-static model was developed to calculate the load distribution in the MCRB, and an optimization model was established to obtain the optimized geometric parameters for a longer fatigue life of the MCRB.

3.1 Quasi-Static Model

The quasi-static model was developed based on the static assumption, where the load–deformation relationship in the MCRB was considered. A schematic of the piston assembly load is shown in Figure 3(a). The piston assembly is subjected to a hydraulic force on the bottom of the piston (F_h), contact force by the guide plate ($F_{1,n}$), and contact force by the cam ring ($F_{2,n}$). The pressure angle between the cam roller and cam ring is $\beta_1 = \beta_n$, whereas the pressure angle between the guide roller and guide plate β_2 can be considered as $\pi/2$. Based on the load balance relationship, $F_{1,n} = F_h \tan(\beta_n) / 2$ and $F_{2,n} = F_h / (2 \cos(\beta_n))$ can be deduced. As shown in Figure 3(b), the component forces of the cam and guide rollers acting on the piston pin are $F_{R,x} = F_{R,n} \sin(\beta_1)$ and $F_{R,z} = F_{R,n} \cos(\beta_2)$, where $R = 1$ refers to the guide roller and $R = 2$ refers to the cam roller in the MCRB. The moments acting on the piston pin were calculated using the deflection angle. According to the Timshenko beam theory, the deflection angle of an arbitrary section of the piston pin in the yo_z plane (θ_x) can be expressed as [33]:

$$EI \frac{d\theta_x}{dy} = \begin{cases} F_{2,z}y - M_{2,x}, & y \in [o_2, o_3], \\ F_{2,z}(y - L_r - L_h) - M_{2,x}, & y \in [o_3, o_4], \end{cases} \quad (1)$$

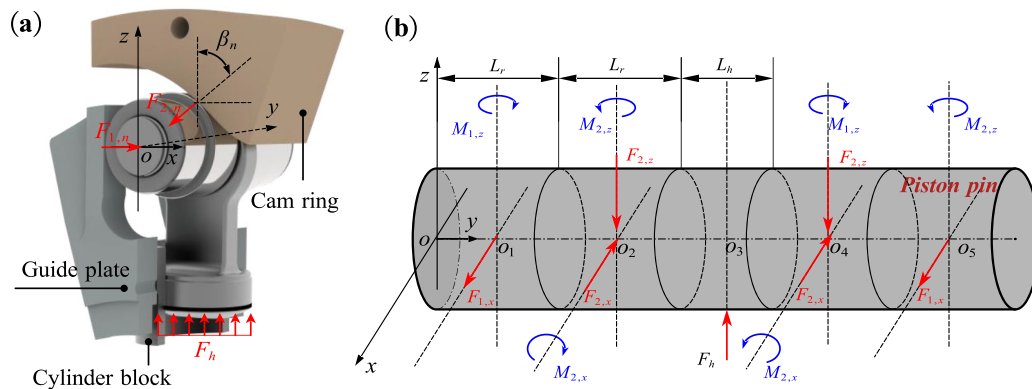


Figure 3 Load analysis of (a) piston assembly and (b) piston pin

where L_r is the outer ring width of the cam and guide rollers. L_h denotes the piston width. E and I are the elastic modulus and moment of inertia of the piston pin, respectively. Considering the antiderivatives of Eq. (1) and the continuity condition of the piston pin deflection, the moment acting on the piston pin in the yoz plane can be expressed as [12]:

$$M_{2,x} = \frac{F_h}{8} (L_r + L_h) - \frac{EI\theta_{2,px}}{L_r + L_h}, \tag{2}$$

where $\theta_{2,px}$ is the deflection angle at point o_2 , as shown in Figure 3(b). Based on the load-balance relationship of the piston pin, $M_{2,n} = M_{2,x} / \cos(\beta_2)$, $M_{2,z} = M_{2,x} \tan(\beta_2)$, and $M_{1,z} = M_{2,z}$ can be deduced.

Figure 4(a) shows the overall load schematic of a cam roller or guide roller under a normal contact load ($F_{R,n}$, $M_{R,n}$) with a pressure angle β_R , where $R = 1$ refers to the guide roller and $R = 2$ refers to the cam roller in the MCRB. The reaction loads generated on the piston pin are $F_{R,x}$, $M_{R,x}$, $F_{R,z}$ and $M_{R,z}$. Figure 4(b) shows the cross-section of the outer ring along the normal direction. As the outer ring is in line with the cam ring or guide plate, the normal contact load ($F_{R,n}$, $M_{R,n}$) can be calculated using the slicing technique. The outer ring is divided into n_r slices; thus, the length coordinate of the k_n th slice is $y_{kn} = -L_r/2 + (k_n - 1/2)L_r/n_r$. Then, the contact force on the k_n th slice of the outer ring can be calculated using Hertzian contact theory:

$$q_{R,kn} = c_r \delta_{R,kn}^{10/9}, \tag{3}$$

where c_r denotes the contact stiffness between the outer ring and the cam ring/guide plate [6]. $\delta_{R,kn}$ is the contact

interference between the outer ring and the cam ring/guide plate, which is related to the microdisplacement of the outer ring. Then, the normal contact load ($F_{R,n}$, $M_{R,n}$) can be calculated as:

$$\begin{cases} \sum_{k_n=1}^{n_r} q_{R,kn} - F_{R,n} = 0, \\ \sum_{k_n=1}^{n_r} y_{kn} q_{R,kn} - M_{R,n} = 0. \end{cases} \tag{4}$$

Figure 4(c) shows the cross-section of the j th needle at an azimuth angle of ψ_j , where $\psi_j = 2\pi(j-1)/n_b$ and n_b is the total number of needles. Considering the cam and guide rollers are both fully complemented needle bearings, the total needle number can be calculated as follows [34]:

$$n_b = \text{fix} \left(\frac{\pi}{\arcsin(d_r/d_m)} \right). \tag{5}$$

The function $\text{fix}(\cdot)$ rounds the argument to the nearest integer towards zero. The needle is divided into n_s slices; thus, the length coordinate of the k th slice is $y_k = -l_r/2 + (k - 1/2)l_r/n_s$, l_r is the needle length. Then, the contact force on the k th slice of the j th needle can be calculated using the Hertz contact theory:

$$q_{R,ijk} = c_s \delta_{R,ijk}^{10/9}, \tag{6}$$

$$q_{R,ojk} = c_s \delta_{R,ojk}^{10/9}, \tag{7}$$

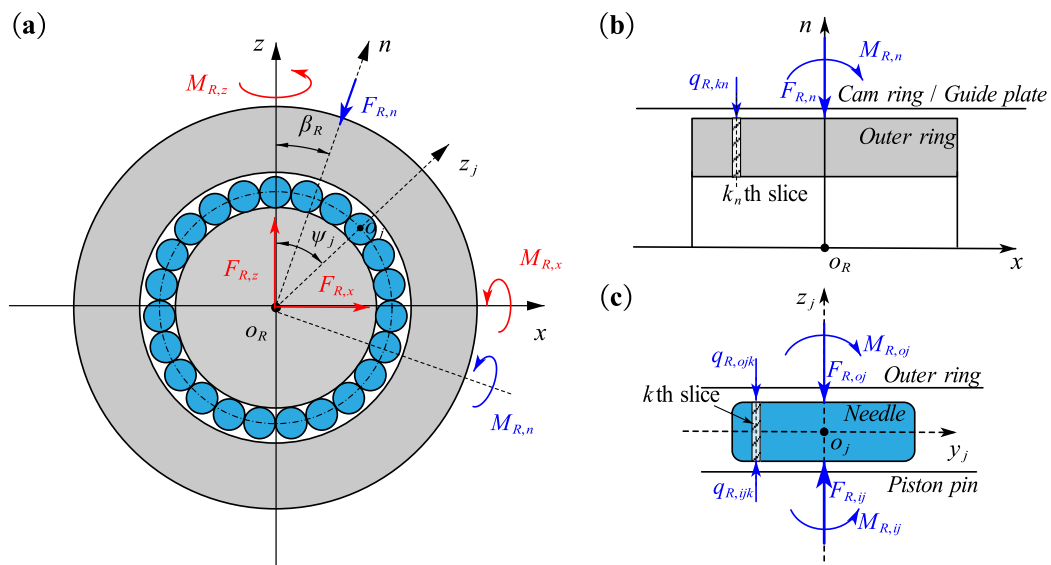


Figure 4 Load analysis on the MCRB: (a) Load on the whole MCRB, (b) Load on the outer ring, (c) Load on the needle

where c_s is the contact stiffness between the needle and outer ring/piston pin. $\delta_{R,ijk}$ and $\delta_{R,ojk}$ are the contact interferences between the needle and the outer ring/piston pin—related to the microdisplacements of the piston pin and needle. This calculation method is described in detail elsewhere [32]. The contact forces and moments on the j th needle can be calculated using $F_{R,ij} = \sum_{k=1}^{n_s} q_{R,ijk}$, $F_{R,oj} = \sum_{k=1}^{n_s} q_{R,ojk}$, $M_{R,ij} = \sum_{k=1}^{n_s} y_k q_{R,ijk}$, and $M_{R,oj} = \sum_{k=1}^{n_s} y_k q_{R,ojk}$. Then, the equilibrium equation of the j th needle can be expressed as:

$$\begin{cases} F_{R,ij} + F_{R,cj} - F_{R,oj} = 0, \\ M_{R,ij} - M_{R,oj} = 0, \end{cases} \quad (8)$$

where $F_{R,cj}$ is the centrifugal force of the j th needle on the cam and guide rollers, respectively. For the load equilibrium of the entire cam or guide roller, the equilibrium equation can be expressed as:

$$\begin{cases} \sum_{j=1}^{n_b} (F_{R,ij} \sin(\psi_j)) - F_{R,x} = 0, \\ \sum_{j=1}^{n_b} (F_{R,ij} \cos(\psi_j)) - F_{R,z} = 0, \\ \sum_{j=1}^{n_b} (M_{R,ij} \cos(\psi_j)) - M_{R,x} = 0, \\ \sum_{j=1}^{n_b} (M_{R,ij} \sin(\psi_j)) - M_{R,z} = 0. \end{cases} \quad (9)$$

In a cam or guide roller, the outer ring deformation, which can significantly affect the load distribution, can be calculated as:

$$u_{R,f}(\varphi) = \sum_{j=1}^{n_b} K_r(\varphi, \psi_j) F_{R,oj} - K_r(\varphi, \beta_R) F_{R,n}, \quad (10)$$

where K_r is the Fourier series estimated using [35]. φ is an arbitrary positional angle of the outer ring.

The microdisplacements of the piston pin, needles, and outer ring in the cam and guide rollers were obtained by solving Eq. (4) and Eqs. (8)–(10). The iterative Newton–Raphson method is used. The contact forces on each slice of the needles ($q_{R,ijk}$, $q_{R,ojk}$) in the cam and guide rollers can then be obtained. Based on the Hertz theory, the contact pressure between the needles and the piston pin/outer ring ($p_{R,ijk}$, $p_{R,ojk}$) can be calculated as:

$$p_{R,ajk} = \sqrt{\frac{q_{R,ajk} n_b E'}{\pi l_r} \left(\frac{1}{d_r} + \frac{1}{d_m \mp d_r} \right)}, \quad (11)$$

where E' is the equivalent elastic modulus. $a = i$ is the upper sign, indicating the contact between the needle and piston pin. $a = o$ is the lower sign, referring to the contact between the needle and outer ring.

3.2 Optimization Model

The objective of the MCRB optimization method is to prolong the fatigue life by optimizing the geometric parameters. The fatigue life of the MCRB was calculated using the load distribution and basic dynamic load rating. The basic dynamic load rating of the cam and guide rollers in the MCRB can be expressed by the following geometric parameters [28]:

$$C_r = b_m f_c (i l_r)^{\frac{7}{9}} n_b^{\frac{3}{4}} d_r^{\frac{29}{27}}, \quad (12)$$

with

$$f_c = 172.5 \frac{\gamma^{\frac{2}{9}} (1 - \gamma)^{\frac{29}{27}}}{(1 + \gamma)^{\frac{1}{4}}} \left\{ 1 + \left[1.038 \left(\frac{1 - \gamma}{1 + \gamma} \right)^{\frac{143}{108}} \right]^{9/2} \right\}^{-2/9}, \quad (13)$$

where i denotes the number of rows of the cam and guide rollers. b_m is a modification factor for improving the quality of the bearing steel; $b_m = 1.1$. γ is an auxiliary parameter, defined as $\gamma = d_r / d_m$.

The dynamic load rating of the piston pin or outer ring can be calculated as follows:

$$Q_{ci} = \frac{1}{0.83} \frac{C_r}{0.378 n_b (\cos \alpha) i^{7/9}} \left\{ 1 + \left[1.038 \left(\frac{1 - \gamma}{1 + \gamma} \right)^{\frac{143}{108}} \right]^{9/2} \right\}^{-2/9}, \quad (14)$$

$$Q_{co} = \frac{1}{0.83} \frac{C_r}{0.364 n_b (\cos \alpha) i^{7/9}} \left\{ 1 + \left[1.038 \left(\frac{1 - \gamma}{1 + \gamma} \right)^{\frac{143}{108}} \right]^{-9/2} \right\}^{2/9}, \quad (15)$$

where α is the nominal contact angle and $\alpha = 0$.

Then, the basic dynamic load rating of a single contact slice of the raceway is:

$$q_{cak} = Q_{ca} \left(\frac{1}{n_s} \right)^{\frac{7}{9}} \tag{16}$$

The equivalent contact pressure concentrated on the k th slice of the j th needle is [13]:

$$q_{R,eak} = \left(\frac{1}{n_b} \sum_{j=1}^{n_b} \left(\left(\frac{p_{R,ajk}}{271} \right)^2 d_r (1 \mp \gamma) \frac{l_r}{n_s} \right)^w \right)^{1/w} \tag{17}$$

where $w = 4$ for the rotating ring, i.e., the outer ring, and $w = 4.5$ for the nonrotating ring, i.e., the piston pin.

Finally, the fatigue life of the guide and cam rollers in the MCRB was calculated based on ISO/TS 16281 [6].

$$L_{R,10r} = \left(\sum_{k=1}^{n_s} \left(\left(\frac{q_{cik}}{q_{R,eik}} \right)^{-9/2} + \left(\frac{q_{cok}}{q_{R,eok}} \right)^{-9/2} \right) \right)^{-8/9} \tag{18}$$

where $R = 1$ refers to the guide roller and $R = 2$ refers to the cam roller.

According to the load analysis in Section 3.1, the external contact force on the cam roller ($F_{2,n}$) was generally smaller than that on the guide roller ($F_{1,n}$). Therefore, the fatigue life of the cam roller is generally shorter than that of the guide roller. Therefore, the fatigue life of the cam roller was set as the objective function. The needle diameter (d_r) and pitch diameter (d_m) are the basic geometric parameters of the MCRB that determine the fatigue life and can be selected as design variables. The other geometric parameters and working conditions are listed in Table 1. Thus, the objective function can be expressed as:

$$\max [f(d_r, d_m)] = \max (L_{2,10r}). \tag{19}$$

The constraints of the optimization model are as follows: First, the fatigue life of the guide rollers $L_{1,10r}$ should be no less than that of the cam rollers $L_{2,10r}$ during

the geometry optimization of the MCRB. In addition, variations in the geometric parameters can lead to a high contact pressure between the needles and raceways, possibly resulting in some degree of permanent deformation at the contact surfaces. To avoid this type of failure, the contact pressure should be constrained to less than 4000 MPa [28]. Furthermore, variations in the needle diameter (d_r) and pitch diameter (d_m) can also change the thickness of the outer rings and the diameter of the crosshead pin, which significantly influences the strength of these parts. The maximum stress in the outer ring of the cam roller $S_{1,r}$, maximum stress in the outer ring of the guide roller $S_{2,r}$, and maximum stress in the piston pin S_c should be less than the permissible yield stress $[\sigma_m]$. Finally, the circumference clearance C between the needles should be larger than the limited value C_{LV} to guarantee the smooth running of the needles without collision—generally one degree between needles [28].

In summary, the optimization constraints are:

$$\begin{cases} L_{1,10r} \geq L_{2,10r}, \\ \max(p_{R,ajk}) \leq 4000 \text{ MPa}, \\ S_{R,r} \leq [\sigma_m], \\ S_c \leq [\sigma_m], \\ C - C_{LV} \geq 0. \end{cases} \tag{20}$$

A computer program was developed to calculate the objective functions and constraints using MATLAB and then linked to commercial optimization software. A genetic optimization algorithm was applied to determine the optimal solution. A flowchart of the optimization procedure is presented in Figure 5. The principle of the genetic optimization method can be expressed as an analogy between natural selection and the survival of fitness. Genetic optimization starts with a randomly generated population of individuals. Individuals in the initial population are characterized by genomes containing a string of chromosomes (randomly generated design variables). The evaluation process follows, in which each individual is evaluated based on the fitness function expressed in terms of the objective function. Using natural genetic operators, selection, crossover, and mutation are used to update a population [36]. Finally, the optimized design variables were obtained.

4 Optimization Results and Discussion

The initial design and ranges of the design variables are listed in Table 2. In total, 1000 designs were calculated, and the computation time for a single design was approximately 0.2 s. The optimization curves of the design variables and objectives are plotted in Figure 6(a) and (b), respectively. First, random designs of experiment (DOE) were created as the initial population for the optimization

Table 1 Basic parameters in geometry optimization

Nomenclature	Value
Needle length l_r	26 mm
Total needle number n_b	Calculated by Eq. (5)
Width of the cam roller and guide roller L_r	32.5 mm
Width of the piston L_h	26 mm
Outer ring diameter of the guide roller D_1	75 mm
Outer ring diameter of the cam roller D_2	85 mm
Elastic modulus of the piston pin E	206 GPa
Equivalent elastic modulus E'	226 GPa
Hydraulic force F_h (hydraulic pressure)	141.8 kN (25 MPa)
Pressure angle β_n	35°

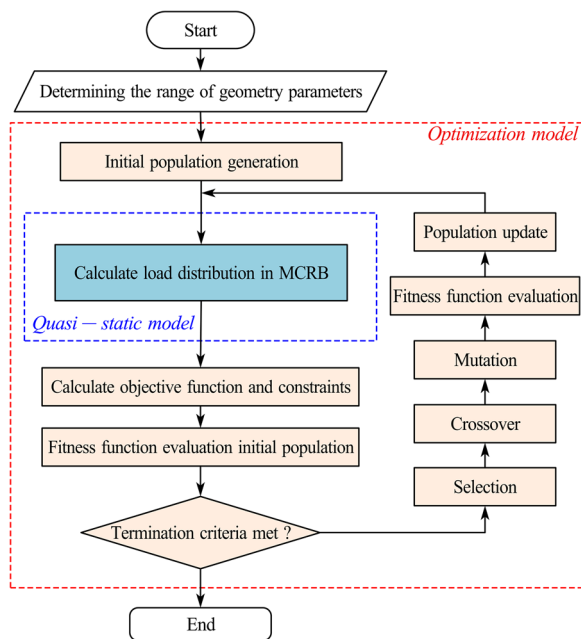


Figure 5 Flowchart of the geometry optimization method

Table 2 Range of the design variables

Value	Needle diameter d_r (mm)	Pitch diameter d_m (mm)
Initial value	6	48
Lower bound	1	20
Upper bound	20	70
Optimized	7.87	52.91

algorithms. Then, the variation in the design variables and the objective tends to stabilize after approximately 400 generations. After optimization, the fatigue of the cam rollers in MCRB increased from 0.66×10^6 to 1.31×10^6 r (approximately 98.5% increase), while the fatigue life of the guide rollers in MCRB increased from 4.29×10^6 to 6.82×10^6 r (approximately 59.0% increase), thus indicating that the proposed optimization method can effectively improve the fatigue life of MCRB. Generally, the MCRB is the first to fail in hydraulic motors. Thus, this optimization method can effectively prolong the fatigue life of hydraulic motors.

Figure 7(a) and (b) show the contact pressure distributions in the initial and optimized guide rollers, respectively, and Figure 7(c) presents the contact pressure along the length of the most loaded needle. The contact pressure distributions of the initial and optimized guide rollers were similar, indicating that the optimization method did not increase the contact pressure on the guide rollers. Figure 8 shows the contact pressure distributions in the initial and optimized cam rollers. The maximum contact pressure in the optimized cam roller is significantly lower than that in the initial one. Therefore, the optimization method can reduce the contact pressure in the MCRB. According to Eq. (12), the basic dynamic load rating of the optimized guide and cam rollers in the MCRB increased from 89 to 109 kN. As a result, the fatigue life of both the guide and cam rollers increased. In summary, the optimization method increased the fatigue life of the MCRB by reducing the contact pressure and increasing the dynamic load ratings.

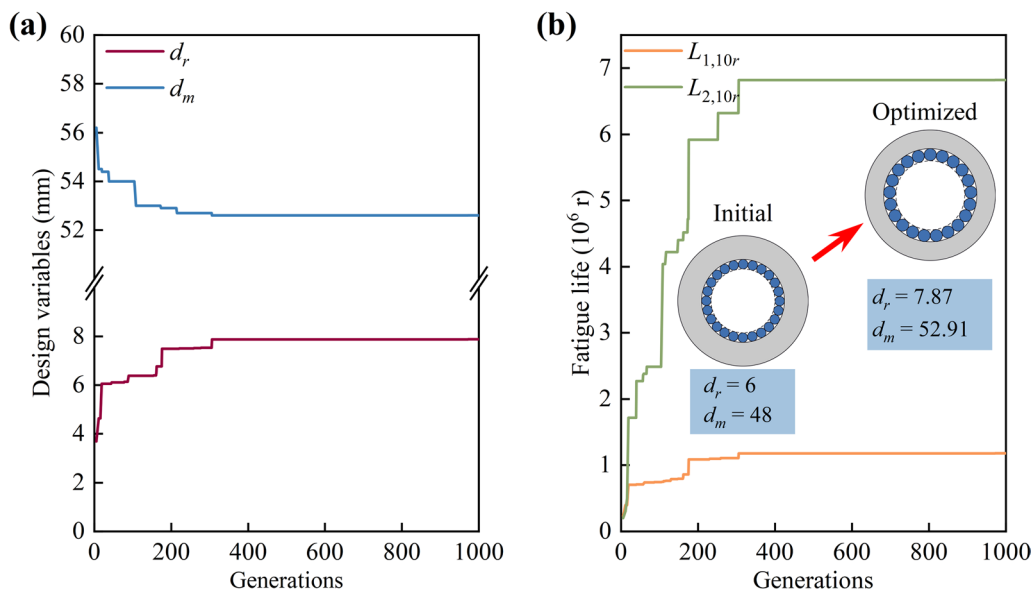


Figure 6 Optimized curves of (a) design variables and (b) the objective function

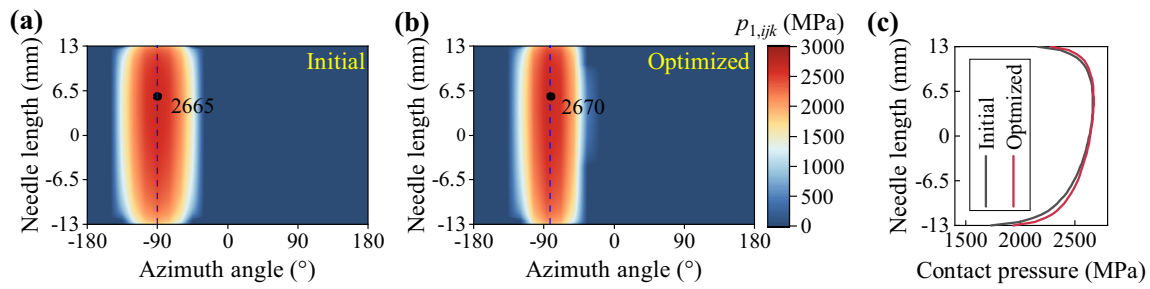


Figure 7 Comparison of contact pressure distribution in the guide roller: (a) Initial guide roller, (b) Optimized guide roller, (c) Most loaded needle in the initial and optimized guide roller

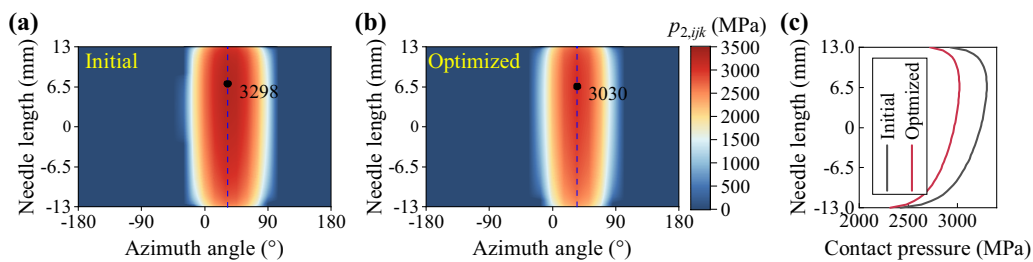


Figure 8 Comparison of contact pressure distribution in the cam roller: (a) Initial cam roller, (b) Optimized cam roller, (c) Most loaded needle in the initial and optimized cam roller

5 Experimental Validation

The full fatigue life test of an MCRB in a hydraulic motor is time-consuming. It is difficult to identify when the MCRB starts fatiguing because it is assembled in the motor and difficult to observe during the test. However, the fatigue life of an MCRB depends on its basic dynamic load rating and distribution. The dynamic load rating of the optimized MCRB, which was calculated using geometric parameters, improved from 89 to 109 kN. Therefore, a reduction in the contact pressure is an alternative way to prove the effectiveness of the proposed geometry optimization method. In this study, a loading test was conducted on a hydraulic motor installed with both initial and optimized MCRB. The wear losses of the initial and optimized MCRB were compared to demonstrate the contact pressure reduction in the optimized MCRB, thereby validating the proposed optimization method indirectly.

Four piston assemblies each, with the initial MCRB and the optimized MCRB, were manufactured. Figure 9 presents the material preparation procedure used in the experiment. The initial and optimized cam and guide rollers are shown in Figure 9(a). Then, the corresponding piston and piston pins were prepared and assembled, as shown in Figure 9(b) and (c). Next, the cam rollers, guide rollers, and other parts were mounted

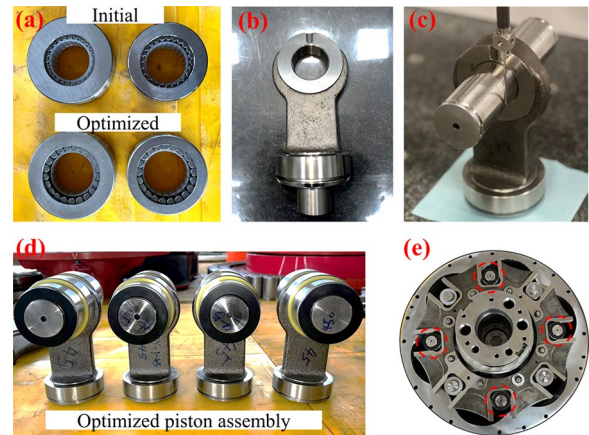


Figure 9 Material preparation for the experiment: (a) Initial and optimized cam roller and guide roller, (b) Piston, (c) Piston and piston pin, (d) Optimized piston assembly, (e) Hydraulic motor

on the piston pin, as shown in Figure 9(d). Finally, four piston assemblies with the initial MCRB and four with the optimized MCRB were assembled in the hydraulic motor, as shown in Figure 9(e). The initial and optimized piston assemblies are arranged alternately in the tested hydraulic motor, whereas the optimized piston assemblies are marked by red circles in Figure 9(e).

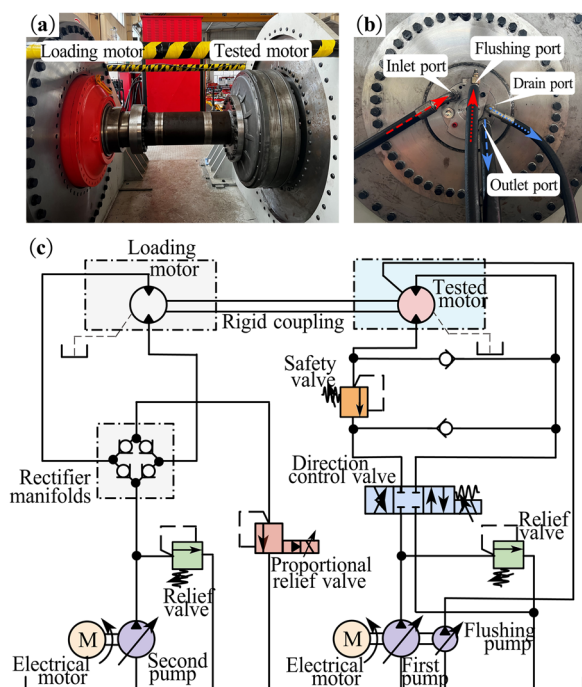


Figure 10 Hydraulic motor test bench: (a) Front view of the test bench, (b) Side view of the tested motor, (c) Schematic of the test bench hydraulic system

The hydraulic motor test bench is shown in Figure 10. The output shafts of the two hydraulic motors with similar displacements were rigidly coupled. The tested motor was actuated using the first pump with a high-pressure oil output. The loading motor serves as a pump, where low-pressure oil is pumped by the second pump, which then outputs high-pressure oil. The outlet pressure of the loading motor and the inlet pressure of the tested motor were adjusted using a proportional relief valve. The

rotational speeds of the two motors were adjusted based on the displacement of the first and second pumps.

Before and after the experiment, the circular profile of the prepared piston pins was measured using a CMM, as shown in Figure 9(c). The CMM used in this study is Zeiss CMM Micura 5/5/5 with a measuring accuracy of less than 1 μm. During the measurements, five uniformly spaced circles along the contact length between the cam roller and the piston pin in each piston assembly were selected and measured.

The experimental operating conditions are shown in Figure 11(a). The duration of the experiment was approximately 6 h. The inlet pressure of the tested motor was varied from 15 to 25 MPa (equivalent to a hydraulic force F_h of 85 to 141.8 kN), and the rotation speed was varied from 15 to 10 r/min. After the hydraulic motor test bench experiment, the piston pin was measured again to calculate the circular wear loss. The wear loss results are shown in Figure 11(b). The wear loss in the optimized MCRB was much smaller than that in the initial MCRB, indicating significant reductions in the contact pressures in the optimized MCRB. The average reduction rate was approximately 60%. Consequently, the fatigue life of the MCRB was improved using the proposed optimization method.

6 Conclusions

In this study, an innovative geometry optimization method for the MCRB to improve the fatigue life of hydraulic motors was proposed. A loading test was conducted on a hydraulic motor installed with both the initial and optimized MCRB to validate the effectiveness of the proposed optimization method. The following conclusions were drawn.

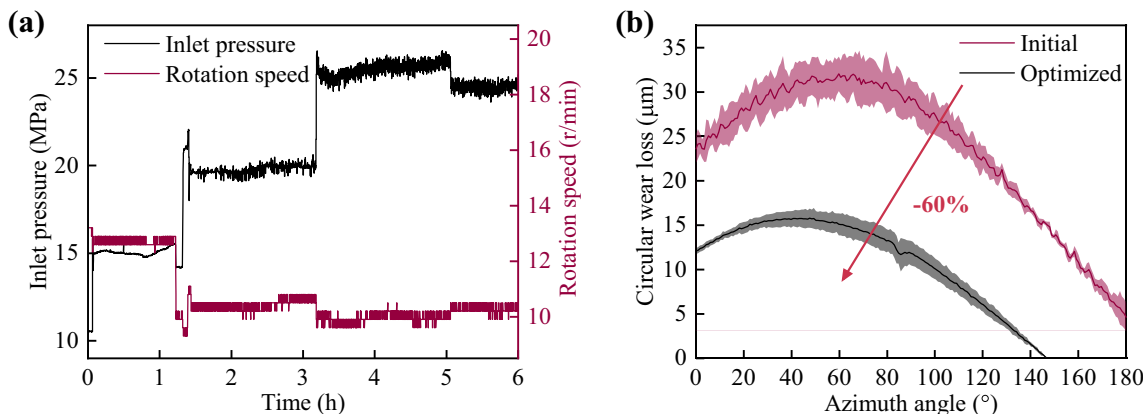


Figure 11 Experimental condition and results: (a) Working conditions of the tested motor, (b) Measurement results of the initial and optimized piston pins

- (1) The proposed geometry optimization method can effectively increase the fatigue life of the MCRB in hydraulic motors: Approximately 98.5% increase for the cam roller and approximately 59.0% increase for the guide roller.
- (2) The fatigue life of an MCRB is based on its basic dynamic load rating and distribution. The proposed geometry optimization method can reduce the contact pressure and improve the basic dynamic load rating of the MCRB, thereby increasing the fatigue life.
- (3) The experimental results showed that the wear loss of the piston pin on the optimized MCRB could be reduced by approximately 60%, indicating that the contact pressures in the optimized MCRB were significantly smaller than those in the initial one. Thus, indirectly validating the improvement in the fatigue life of the optimized MCRB is possible.

While geometry optimization is an effective method for improving the fatigue life of MCRB in hydraulic motors, it has limitations. The geometry optimization design can approach material performance limit continuously, but can not exceed it. In future work, a fatigue life test rig of the MCRB will be established, particularly focusing on material surface strengthening in the MCRB to further improve the fatigue life.

Acknowledgments

Not applicable.

Authors' Contributions

JZ, BX, and QS were responsible for the entire trial; YF was a major contributor in writing the manuscript; PD, YY, and CZ assisted in the experiment. All authors read and approved the final manuscript.

Funding

Supported by National Key R&D Program of China (Grant No. 2021YFB3400501).

Data availability

Not applicable.

Declarations

Competing interests

The authors declare no competing financial interests.

Received: 16 October 2023 Revised: 17 July 2024 Accepted: 22 July 2024

Published online: 15 August 2024

References

- [1] C Zhang, H Tan, Y Fang, et al. Deformation pre-compensated optimization design of cam ring for low pulsation hydraulic motors. *Journal of Zhejiang University-SCIENCE A*, 2023, 24(2): 130–145.
- [2] J K Woodacre, R J Bauer, R Irani. Hydraulic valve-based active-heave compensation using a model-predictive controller with non-linear valve compensations. *Ocean Engineering*, 2018, 152: 47–56.
- [3] F Wang, J Chen, M Cheng, et al. A novel hydraulic transmission solution to large offshore wind turbine: Design and control strategy. *Ocean Engineering*, 2022, 255: 111285.
- [4] D Nilsson, B Prakash. Investigation into the seizure of hydraulic motors. *Tribology International*, 2010, 43: 92–99.
- [5] M Shirzadegan, A Almqvist, R Larsson. Fully coupled EHL model for simulation of finite length line cam-roller follower contacts. *Tribology International*, 2016, 103: 584–598.
- [6] International Organization for Standardization. ISO/TS 16281: 2008 Rolling Bearings—Methods for Calculating the Modified Reference Rating Life for Universally Loaded Bearings, 2008.
- [7] S W Hong, V C Tong. Rolling-element bearing modeling: A review. *International Journal of Precision Engineering and Manufacturing*, 2016, 17(12): 1729–1749.
- [8] L Kania. Modelling of rollers in calculation of slewing bearing with the use of finite elements. *Mechanism and Machine Theory*, 2006, 41(11): 1359–1376.
- [9] N Demirhan, B Kanber. Stress and displacement distributions on cylindrical roller bearing rings using FEM. *Mechanics Based Design of Structures and Machines*, 2008, 36(1): 86–102.
- [10] R Lostado, R F Martinez, B J Mac Donald. Determination of the contact stresses in double-row tapered roller bearings using the finite element method, experimental analysis and analytical models. *Journal of Mechanical Science and Technology*, 2015, 29(11): 4645–4656.
- [11] A B Jones. A general theory for elastically constrained ball and radial roller bearings under arbitrary load and speed conditions. *Journal of Basic Engineering*, 1960, 82(2): 309–320.
- [12] T A Harris, M N Kotzalas. *Advanced concepts of bearing technology: Rolling bearing analysis*. Boca Raton: CRC Press, 2006.
- [13] V Ivannikov, M Leontiev, S Degtyarev, et al. Analysis of radial roller bearing rating life in complex loading conditions. *Journal of Tribology*, 2022, 144(3): 031201.
- [14] L H Zhao, Q C Li, J Z Feng, et al. Service life prediction method for wheel-hub-bearing under random multi-axial wheel loading. *Engineering Failure Analysis*, 2021, 122: 105211.
- [15] Z Jiang, X Huang, H Zhu, et al. A new method for contact characteristic analysis of the tapered roller bearing in wind turbine main shaft. *Engineering Failure Analysis*, 2022, 141: 106729.
- [16] J Zheng, J Ji, S Yin, et al. Internal loads and contact pressure distributions on the main shaft bearing in a modern gearless wind turbine. *Tribology International*, 2020, 141: 105960.
- [17] J Liu, H Wu, Y Shao. A theoretical study on vibrations of a ball bearing caused by a dent on the races. *Engineering Failure Analysis*, 2018, 83: 220–229.
- [18] B Fang, S Wan, J Zhang, et al. Research on the influence of clearance variation on the stiffness fluctuation of ball bearing under different operating conditions. *Journal of Mechanical Design*, 2021, 143(2): 023403.
- [19] Y Zhang, B Fang, L Kong, et al. Effect of the ring misalignment on the service characteristics of ball bearing and rotor system. *Mechanism and Machine Theory*, 2020, 151: 103889.
- [20] S Panda, S N Panda, P Nanda, et al. Comparative study on optimum design of rolling element bearing. *Tribology International*, 2015, 92: 595–604.
- [21] A Abbasi, B Firouzi, P Sendur, et al. Multi-strategy Gaussian Harris hawks optimization for fatigue life of tapered roller bearings. *Engineering with Computers*, 2022, 38(5): 4387–4413.
- [22] A Baklouti, K Dammak, A E Hami. Optimum reliable design of rolling element bearings using multi-objective optimization based on C-NSGA-II. *Reliability Engineering & System Safety*, 2022, 223: 108508.
- [23] B R Rao, R Tiwari. Optimum design of rolling element bearings using genetic algorithms. *Mechanism and Machine Theory*, 2007, 42(2): 233–250.
- [24] K S Kumar, R M P Tiwari, P Prasad. An optimum design of crowned cylindrical roller bearings using genetic algorithms. *Journal of Mechanical Design*, 2009, 131(5): 051011.
- [25] R Tiwari, R Chandran. Multitude of objectives based optimum designs of cylindrical roller bearings with evolutionary methods. *Journal of Tribology*, 2015, 137(4): 041504.
- [26] M Kalyan, R Tiwari. Multi-objective optimization of needle roller bearings based on fatigue and wear using evolutionary algorithm. *Proceedings of the Institution of Mechanical Engineers, Part J: Journal of Engineering Tribology*, 2016, 230(2): 170–185.

- [27] S K Verma, R Tiwari. Robust optimum design of tapered roller bearings based on maximization of fatigue life using evolutionary algorithm. *Mechanism and Machine Theory*, 2020, 152: 103894.
- [28] V Waghole, R Tiwari. Optimization of needle roller bearing design using novel hybrid methods. *Mechanism and Machine Theory*, 2014, 72: 71–85.
- [29] S W Kim, K Kang, K Yoon, et al. Design optimization of an angular contact ball bearing for the main shaft of a grinder. *Mechanism and Machine Theory*, 2016, 104: 287–302.
- [30] J Liu, Z Xu. An optimization design method of a cylindrical roller bearing with the low friction torque. *Journal of Tribology*, 2022, 144(11): 111201.
- [31] K Kang, S W Kim, K Yoon, et al. Robust design optimization of an angular contact ball bearing under manufacturing tolerance. *Structural and Multidisciplinary Optimization*, 2019, 60(4): 1645–1665.
- [32] Y Fang, C Zhang, C Xu, et al. Combined influence mechanism of the flexible free outer ring on contact characteristic in heavy-load cam roller bearings. *Engineering Failure Analysis*, 2024, 156: 107835.
- [33] E Carrera, G Giunta, M Petrolo. *Beam structures: Classical and advanced theories*. John Wiley & Sons, 2011.
- [34] C Ursache, A Barili, L Tudose, et al. Optimal design of self-retaining full complement cylindrical roller bearings. *IOP Conference Series: Materials Science and Engineering*, 2019, 659(1): 012065.
- [35] Y Mao, L Wang, C Zhang. Influence of ring deformation on the dynamic characteristics of a roller bearing in clearance fit with housing. *International Journal of Mechanical Sciences*, 2018, 138: 122–130.
- [36] C M Chan, H L Bai, D Q He. Blade shape optimization of the Savonius wind turbine using a genetic algorithm. *Applied Energy*, 2018, 213: 148–157.

Yu Fang born in 1999, is currently a Ph.D. candidate at *State Key Laboratory of Fluid Power and Mechatronic Systems, Zhejiang University, China*. His research interests include hydraulic motors and rolling contact mechanics.

Qi Su born in 1987, is currently an assistant research fellow at *State Key Laboratory of Fluid Power and Mechatronic Systems, Zhejiang University, China*. He received his Ph.D. degree from *Zhejiang University, China*, in 2016. His primary research interests include electromechanical systems and hydraulic valves.

Pengpeng Dong born in 1986, is currently an engineer at *Hangzhou Applied Acoustics Research Institute, China*.

Yu Yang born in 1978, is currently an engineer at *Zenmax Hydraulics Co., Ltd, China*.

Bing Xu born in 1971, is a professor at *Zhejiang University, China*. He served as a director at *State Key Laboratory of Fluid Power and Mechatronic Systems, Zhejiang University, China*. His main research interests include hydraulic components and systems.

Chao Zhang born in 1990, is currently a research fellow at *State Key Laboratory of Fluid Power and Mechatronic Systems, Zhejiang University, China*. His primary research interests include the design and manufacture of hydraulic motors.

Junhui Zhang born in 1983, is currently deputy director at *State Key Laboratory of Fluid Power and Mechatronic Systems, Zhejiang University, China*. He received his Ph.D. degree from *Zhejiang University, China*, in 2012. His research interests include hydraulic transmissions, hydraulic components, and hydraulic robots.